Determination of rotational alignment of $N_2^+ B\,^2\Sigma_u^+$ and $CO^+ B\,^2\Sigma^+$ following photoionization of N_2 and CO

J. A. Guest, K. H. Jackson,* and R. N. Zare
Department of Chemistry, Stanford University, Stanford, California 94305
(Received 1 June 1983)

When a low-pressure (10^{-2}-Torr) sample of N_2 or CO is exposed to a beam of linearly polarized synchrotron radiation (18—34 eV), electronically excited molecular ions are formed whose subsequent unresolved emission is found to be partially polarized. The degree of polarization of the $N_2^+ B\,^2\Sigma_u^+$-$X\,^2\Sigma_g^+$ fluorescence ($\sim$391 nm) and the $CO^+ B\,^2\Sigma^+$-$X\,^2\Sigma^+$ fluorescence ($\sim$220 nm) is studied as a function of the energy of the ionizing radiation from threshold to higher energies. This information determines the alignment of the photoion, which in the case of N_2 must be corrected for depolarization caused by spin-rotation and hyperfine interaction. From the polarization of the fluorescence we deduce γ, the ratio of parity-unfavored to the sum of parity-favored contributions for photoelectron ejection. Comparison of the dynamical channel ratio γ with theoretical calculations for σ- and π-photoelectron ejection shows poor agreement for N_2 and fair agreement for CO.

I. INTRODUCTION

Photoionization of an atomic or molecular target by interaction with a beam of light is well known to be an inherently anisotropic process.[1,2] This anisotropy can manifest itself in two ways: (1) through the angular distribution of the photoelectron described by the β parameter ($-1 \le \beta \le 2$) (Refs. 3—5) and (2) through the alignment and/or orientation of the residual target ion.[6—10] When the target ion is formed in an excited electronic state, then the alignment and/or orientation is readily determined by measuring the degree of polarization of the resulting target ion fluorescence. By this means Poliakoff *et al.*[10] first demonstrated molecular photoion alignment using the Synchrotron Ultraviolet Radiation Facility (SURF-II) storage ring of the U.S. National Bureau of Standards to photoionize N_2 by removal of an inner σ_u $2s$ electron. The process may be described as

$$N_2(1\sigma_g^2 1\sigma_u^2 2\sigma_g^2 2\sigma_u^2 1\pi_g^4 3\sigma_g^2)X\,^1\Sigma_g^+ + h\nu \rightarrow N_2^+(1\sigma_g^2 1\sigma_u^2 2\sigma_g^2 2\sigma_u 1\pi_g^4 3\sigma_g^2)B\,^2\Sigma_u^+ + e^-(\epsilon\sigma_g,\epsilon\pi_g)$$

followed by

$$N_2^+(1\sigma_g^2 1\sigma_u^2 2\sigma_g^2 2\sigma_u 1\pi_g^4 3\sigma_g^2)B\,^2\Sigma_u^+ \rightarrow N_2^+(1\sigma_g^2 1\sigma_u^2 2\sigma_g^2 2\sigma_u^2 1\pi_g^4 3\sigma_g)X\,^2\Sigma_g^+ + h\nu'(391\text{ nm})\,.$$

From the degree of polarization it is possible to estimate the ratio of cross sections for the two degenerate $(\epsilon\sigma_g,\epsilon\pi_g)$ ionization pathways. However, this analysis requires that the spectroscopy of the ion fluorescence is understood.

We present here a continuation of these experiments which have been carried out over a broader energy range, including threshold, using the Stanford Synchrotron Radiation Laboratory (SSRL) vacuum ultraviolet (vuv) source. In addition, these experiments have been extended to the analogous photoionization process for the isoelectronic carbon monoxide molecule:

$$CO(1\sigma^2 2\sigma^2 3\sigma^2 4\sigma^2 1\pi^4 5\sigma^2)X\,^1\Sigma^+ + h\nu \rightarrow CO^+(1\sigma^2 2\sigma^2 3\sigma^2 4\sigma 1\pi^4 5\sigma^2)B\,^2\Sigma^+ + e^-(\epsilon\sigma,\epsilon\pi)$$

followed by

$$CO^+(1\sigma^2 2\sigma^2 3\sigma^2 4\sigma 1\pi^4 5\sigma^2)B\,^2\Sigma^+ \rightarrow CO^+(1\sigma^2 2\sigma^2 3\sigma^2 4\sigma^2 1\pi^4 5\sigma)X\,^2\Sigma^+ + h\nu'(\sim 220\text{ nm})\,.$$

In both cases emission from the resulting excited molecular ion is found to be partially polarized. The degree of linear polarization is studied as a function of the energy of the ionizing radiation.

Upon converting these polarizations to partial channel ratios, we obtain dynamical information on the photoionization processes that lead to these final excited states. In photoelectron angular distribution studies, the channel ratios are folded together with the phase shift difference of the two outgoing waves.[3—5] As a result dynamical information is more difficult to extract.

The processes that can be studied via measurement of the polarization of the subsequent target fluorescence are those which involve ejection of an inner-shell electron (as in the present case) to yield an electronically excited ion. However, these photoejection processes are difficult to describe theoretically through the use of one-electron models because electron correlation effects are, in general, expected to be important. The quantitative information gained from this study can thus provide clues for the elucidation of these inner-shell events.

Molecular nitrogen has been the subject of numerous experimental[5,11,12] and theoretical[13—16] partial cross-section studies. Nevertheless, the N_2 $2\sigma_u \rightarrow (\epsilon\sigma_g,\epsilon\pi_g)$ differential ejection is poorly understood, in spite of the fact that the photoionization process is known to be primarily direct. Carbon monoxide, because it lacks inversion symmetry, permits additional states in the continuum to couple to-

gether, one of which is a σ (f-wave) shape resonance.[13] The $CO^+ B\,^2\Sigma^+$ cross section peaks at about 32 eV and this behavior is attributed to this $l=3$ resonance.[12,17] Marr *et al.*[5] report no indication that this shape resonance affected their measured electron angular distributions. We present here the first experimental partial channel ratio for CO as a function of the energy of the ionizing radiation. We also find that the observed resonance has the effect of leaving the channel ratio nearly constant as a function of energy.

Quantitative extraction of the partial channel ratios from unresolved photoion fluorescence polarizations is an involved procedure requiring that an average be performed over the rotational alignment functions weighted by emission intensities. We find that a room-temperature gas sample of N_2 results in photoion emission that is necessarily 15–20% less polarized than one would expect for an emitter regarded as a classical Hertzian dipole oscillator. Hyperfine and spin-rotation interaction in the photoion cause the observed alignment to be less than its value in their absence.[8,9,18] The magnitude of the effect is determined by the molecule and the experimental conditions. We apply these corrections to N_2 and CO to extract the "true alignment," i.e., the alignment of the molecular rotation that would occur in the absence of these interactions. The measured polarizations are converted to channel ratios and compared to the best theoretical calculations presently available.

II. THEORY

A. Photoion alignment

Photoion fluorescence polarization can be related to product state alignment (and hence degenerate partial channel ratios) as demonstrated by Greene and Zare (GZ),[8,9] drawing on earlier work by Dill and Fano.[19–21] We present here a summary of these results.

Photoionization continuum channels can be characterized by $\vec{j}_t$, the angular momentum transferred between unobserved photofragments. For Σ symmetry of the parent and the fragment, $\vec{j}_t$ may be defined by

$$\vec{j}_t=\vec{\ell}-\vec{N}=\vec{j}_{ph}-\vec{N}', \tag{1}$$

where $\vec{N}$ is the ground-state rotational angular momentum of the molecule, $\vec{\ell}$ is the orbital angular momentum of the photoelectron, $\vec{j}_{ph}$ is the unit angular momentum coupled to the target by electric-dipole radiation, and $\vec{N}'$ is the rotational angular momentum of the photoion. The electron and nuclear spin of the photoion cannot be aligned in our experiment and these angular momenta are omitted from the definition of $\vec{j}_t$ for simplicity. This transfer formalism leads to cross sections $\sigma(N',M')$ which, for linearly polarized incident light, are an incoherent summation over j_t

$$\sigma(N',M')=\sum_{j_t}|S(N';j_t)|^2(N'M',j_t-M'\,|\,10)^2, \tag{2}$$

where $(N'M',j_t-M'\,|\,10)^2$ is the square of a Wigner coefficient, and $|S(N';j_t)|^2$ is the square of the amplitude for photoionization into the continuum channel characterized by j_t. If the photoelectron escape direction is *not* detected (thus preserving the system's axial symmetry), then polarization of radiation emitted by the photoion is specified in terms of the Fano-Macek (FM) alignment parameter[18]

$$\mathscr{A}_0^{(2)}(N')=\left[\sum_{M'}\sigma(N',M')\frac{3M'^2-N'(N'+1)}{N'(N'+1)}\right]\Big/\sum_{M'}\sigma(N',M') \tag{3}$$

which describes the quadrupole moment of the rotational angular momentum vector $\vec{N}'$.

Since the M' dependence of $\sigma(N',M')$ arises only through Wigner coefficients, the separate contributions of each transfer j_t can be evaluated analytically[8,9]:

$$\mathscr{A}_0^{(2)}(N')=\sum_{j_t}|S(N';j_t)|^2\mathscr{A}_0^{(2)}(N';j_t)\Big/\sum_{j_t}|S(N';j_t)|^2. \tag{4}$$

The Wigner coefficient in Eq. (2) restricts the sum over j_t to the values $N'-1$, N', and $N'+1$. The alignment $\mathscr{A}_0^{(2)}(N')$ is thus an incoherent average of three values of the angular momentum transfer j_t, embodied in the universal alignment function $\mathscr{A}_0^{(2)}(N';j_t)$, the explicit expressions for which are

$$\begin{aligned}\mathscr{A}_0^{(2)}(N';N'+1)&=\frac{-2}{5}+\frac{3}{5(N'+1)},\\ \mathscr{A}_0^{(2)}(N';N')&=\frac{4}{5}-\frac{3}{5N'(N'+1)},\\ \mathscr{A}_0^{(2)}(N';N'-1)&=\frac{-2}{5}-\frac{3}{5N'}.\end{aligned} \tag{5}$$

The experimental polarization

$$P=(I_{\parallel}-I_{\perp})/(I_{\parallel}+I_{\perp}) \tag{6}$$

is computed from the fluorescence intensities $I_{\parallel}$ and $I_{\perp}$, linearly polarized parallel and perpendicular to the electric vector of the incident radiation, respectively. This quantity can be related to the alignment of the excited target ion by

$$P=3h^{(2)}(N',N'')\mathscr{A}_0^{(2)}(N')/[4+h^{(2)}(N',N'')\mathscr{A}_0^{(2)}(N')], \tag{7}$$

where $h^{(2)}(N',N'')$ is a geometrical factor that isolates the effect of the final-state rotational quantum number N'' on the angular distribution of the light emitted by the photoion in the electric dipole process $N'\rightarrow N''$. Explicit evaluation of $h^{(2)}(N',N'')$ gives

$$\begin{aligned} &h^{(2)}(N',N'+1)=-N'/(2N'+3)\,,\\ &h^{(2)}(N',N')=1\,,\\ &h^{(2)}(N',N'-1)=-(N'+1)/(2N'-1)\,. \end{aligned} \tag{8}$$

In Eq. (7) the degree of polarization P is related to the product of $h^{(2)}$ and $\mathscr{A}_0^{(2)}$ in a nonlinear manner. It is useful to introduce instead the polarization anisotropy R, defined by

$$R=(I_{\parallel}-I_{\perp})/(I_{\parallel}+2I_{\perp})\,, \tag{9}$$

which is related to P by $R=2P/(3-P)$. This has the advantage that the dependence of R upon the product of $h^{(2)}$ and $\mathscr{A}_0^{(2)}$ is linear:

$$R(N',N'')=\tfrac{1}{2}h^{(2)}(N',N'')\mathscr{A}_0^{(2)}(N')\,. \tag{10}$$

B. Extraction of dynamical quantities

The preceding development demonstrates that a fluorescence polarization measurement of an $N'\rightarrow N''$ transition can be inverted to yield the rotational quadrupole alignment $\mathscr{A}_0^{(2)}(N')$. Equations (4) and (5) disentangle the photoionization dynamics contained in the amplitudes $|S(N';j_t)|^2$ from geometrical considerations, all of which are included in the alignment functions $\mathscr{A}_0^{(2)}(N';j_t)$. Extraction of useful dynamical information from the $\mathscr{A}_0^{(2)}(N')$ is the primary goal here.

We introduce the angular momentum transfer channel probabilities

$$\begin{aligned} \mathscr{S}_+&=\frac{|S(N';N'+1)|^2}{\sum_{j_t}|S(N';j_t)|^2}\,,\\ \mathscr{S}_0&=\frac{|S(N';N')|^2}{\sum_{j_t}|S(N';j_t)|^2}\,,\\ \mathscr{S}_-&=\frac{|S(N';N'-1)|^2}{\sum_{j_t}|S(N';j_t)|^2}\,, \end{aligned} \tag{11}$$

where $\mathscr{S}_+ + \mathscr{S}_0 + \mathscr{S}_- = 1$. Using the above terms, Eq. (4) can be rewritten as

$$\begin{aligned} \mathscr{A}_0^{(2)}(N')=\mathscr{S}_+\mathscr{A}_0^{(2)}(N';N'+1)+\mathscr{S}_0\mathscr{A}_0^{(2)}(N';N')\\ +\mathscr{S}_-\mathscr{A}_0^{(2)}(N';N'-1)\,. \end{aligned} \tag{12}$$

In this form, then, the $\mathscr{S}_i$ represent all the dynamical information that can be learned in these experiments by measuring the polarization of fluorescence emitted by a photoion.

From Eq. (12) it is clearly not possible, in general, to deduce the individual channel probabilities. As N' increases, however, the terms $\mathscr{A}_0^{(2)}(N;N'+1)$ and $\mathscr{A}_0^{(2)}(N';N'-1)$ approach their limiting value of $-\frac{2}{5}$ and $\mathscr{A}_0^{(2)}(N';N')$ converges to $\frac{4}{5}$. Thus, at high N',

$$\mathscr{A}_0^{(2)}(N')\simeq-\tfrac{2}{5}(\mathscr{S}_++\mathscr{S}_-)+\tfrac{4}{5}\mathscr{S}_0\,. \tag{13}$$

Following GZ, we define the channel ratio

$$\gamma=\frac{\mathscr{S}_0}{\mathscr{S}_++\mathscr{S}_-}\,, \tag{14}$$

which represents the ratio of the parity-unfavored ($j_t=N'$) to the sum of the parity-favored ($j_t=N'\pm1$) contributions to the total photoionization cross section. In the high-N' limit we find that

$$\mathscr{A}_0^{(2)}=\tfrac{2}{5}(2\gamma-1)/(\gamma+1)\,. \tag{15}$$

Equation (15) provides a valuable parametrization of the alignment in terms of a ratio of dynamical channel probabilities. For the lowest values of N', however, Eq. (12) should be applied in full.

C. Depolarization effects

We are interested in finding the rotational quadrupole alignment $\mathscr{A}_0^{(2)}(N')$ of the isolated excited molecular ion. For low N', the observed alignment may need to be corrected for the presence of other angular momenta that couple to $\vec{N}'$ to form the resultant total angular momentum $\vec{F}'$ about which $\vec{N}'$ precesses. For the case at hand, the photoion has an unpaired electron spin $\vec{S}'=\frac{1}{2}$ causing the excited molecular ion to be a $^2\Sigma^+$ state; in the case of $^{14}N_2$ (but not $^{12}C\,^{16}O$) there is also a spin of $\vec{I}'=1$ on each nucleus. As a result of the precession of $\vec{N}'$ about $\vec{F}'$, $\mathscr{A}_0^{(2)}(N')$ oscillates in time, attaining its maximum value at time $t=0$ when the $\vec{N}'$ distribution has been aligned by the photoionization process but the $\vec{S}'$ and $\vec{I}'$ distributions are unaffected, i.e., randomly oriented. In the present study, the spin-rotation and hyperfine interactions are sufficiently large compared to the natural linewidth of the transitions that the precession is rapid, i.e., $\vec{N}'$ precesses many times about $\vec{F}'$ before emission occurs. The alignment thus oscillates rapidly during the radiative lifetime. The fluorescence detector responds to the average alignment $\mathscr{A}_0^{(2)}(N',\text{obs})$, which may be related to the true alignment of $\vec{N}'$, $\mathscr{A}_0^{(2)}(N')$, by

$$\mathscr{A}_0^{(2)}(N',\text{obs})=\mathscr{A}_0^{(2)}(N')\bar{g}^{(2)}(N')\,, \tag{16}$$

where[8,18]

$$\bar{g}^{(2)}(N')=\sum_{J',F'}\frac{(2J'+1)^2(2F'+1)^2}{(2S'+1)(2I'+1)}\times\begin{Bmatrix}F' & F' & 2\\ J' & J' & I'\end{Bmatrix}^2\begin{Bmatrix}J' & J' & 2\\ N' & N' & S'\end{Bmatrix}^2\,. \tag{17}$$

The derivation Eq. (17) assumes Hund's case $b_{\beta J}$ coupling,[22] i.e., $\vec{N}'$ couples first to $\vec{S}'$ to form $\vec{J}'$. This should be distinguished from Hund's case $b_{\beta S}$ coupling, where $\vec{N}'$ couples to the resultant of $\vec{S}'+\vec{I}'$. Equations (16) and (17) will be explicitly applied to the observed

alignment of the $N_2^+ B\,^2\Sigma_u^+$ and $CO^+ B\,^2\Sigma^+$ ions in extracting $\mathscr{A}_0^{(2)}(N')$.

D. Rotational averaging

In the present experiments individual rotational levels are not resolved. Consequently, an average must be taken over all N' weighted by the intensities $I(N',N'')$ of the $N'\rightarrow N''$ transitions. We express

$$\langle R\rangle=\frac{\frac{1}{2}\sum_{N',N''}h^{(2)}(N',N'')\bar{g}^{(2)}(N')\mathscr{A}_0^{(2)}(N')I(N',N'')}{\sum_{N',N''}I(N',N'')} \tag{18}$$

as the polarization anisotropy averaged over all rotational levels and branches. By making the assumption that the true rotational alignment does not vary with N', we can convert an unresolved fluorescence polarization measurement to a true photoion alignment $\mathscr{A}_0^{(2)}$ provided that the rotational emission intensities are approximately known. The approximation of N'-invariant alignment is inaccurate at the lowest N' values, and the total alignments determined this way are 2—3 % off.

We find it conceptually useful to extract the channel ratio γ from a polarization measurement along with the alignment. We introduce the averaged product

$$\langle \mathscr{S}_i\mathscr{R}_i\rangle=\frac{\frac{1}{2}\sum_{N',N''}\mathscr{S}_i h^{(2)}(N',N'')\bar{g}^{(2)}(N')\mathscr{A}_0^{(2)}(N';i)I(N',N'')}{\sum_{N',N''}I(N',N'')}\,, \tag{19}$$

where i denotes parity favoredness, i.e., i is either $+$, 0, or $-$ depending on whether $j_t=N'+1$, N', or $N'-1$, respectively. This allows Eq. (18) to be recast as

$$\langle R\rangle=\langle \mathscr{S}_+\mathscr{R}_+\rangle+\langle \mathscr{S}_0\mathscr{R}_0\rangle+\langle \mathscr{S}_-\mathscr{R}_-\rangle\,. \tag{20}$$

We see that the dependence of $\langle R\rangle$ on the three continuum channel probabilities is complicated because the latter appear within the averages. We make two assumptions: (1) the continuum channel probabilities are independent of rotation and (2) $\mathscr{S}_+=\mathscr{S}_-$. The first assumption should be valid provided that rotational autoionizing resonances are unimportant in the averaging process. The second assumption is necessary at low N' for this development. Then Eq. (20) becomes

$$\langle R\rangle=\frac{1}{(1+\gamma)}[\tfrac{1}{2}(\mathscr{R}_++\mathscr{R}_-)+\gamma\mathscr{R}_0]\,, \tag{21}$$

where γ is the channel ratio defined by Eq. (14) and

$$\mathscr{R}_i=\frac{\frac{1}{2}\sum_{N',N''}h^{(2)}(N',N'')\bar{g}^{(2)}(N')\mathscr{A}_0^{(2)}(N';i)I(N',N'')}{\sum_{N',N''}I(N',N'')}\,. \tag{22}$$

Hence a measurement of the rotationally unresolved polarization anisotropy $\langle R\rangle$ can be related through Eqs. (21) and (22) to the dynamical channel ratio γ which expresses the ratio of parity-unfavored to parity-favored contributions to the photoionization cross section. This forms the basis for extracting dynamical information from our measurements.

The dynamical quantity of interest, γ, can now be determined from the measured polarization anisotropy. By rearranging Eq. (21), we find that

$$\gamma=\frac{\frac{1}{2}(\mathscr{R}_++\mathscr{R}_-)-\langle R\rangle}{\langle R\rangle-\mathscr{R}_0}\,. \tag{23}$$

The terms $\mathscr{R}_+$, $\mathscr{R}_-$, and $\mathscr{R}_0$ are constants for a given photoion emission with a known rotational distribution. Their values determine the maximum and minimum observable polarizations in a particular photoionization experiment. Calculation of the $\mathscr{R}_i$ as defined in Eq. (22) permits quantitative extraction of the channel ratio γ from the measurement of $\langle R\rangle$. The variations in $\mathscr{R}_i$ for different molecular photoions are geometrical in nature. They depend on the photoionization dynamics only insofar as the distribution of N' in the photoion is affected.

III. EXPERIMENTAL

All experiments were performed at SSRL. A MacPherson 1-m Seya-Namioka—type monochromator with an Os-coated 1200-line/mm grating blazed for 54 nm dispersed the incident vuv light from the storage ring. Four focusing mirrors on the beam line assembly enhanced the incident light polarization in the horizontal plane to greater than 97%.[23] The excitation resolution was either 0.28 or 0.90 nm, as noted.

A 150-nm-thick aluminum foil window (Luxel Corp.) separated the sample chamber (10^{-7} Torr base pressure) from the uhv (10^{-9}-Torr) monochromator. The grating and window combination provided continuously tunable light from 17.5—33 eV (71—37 nm) with relative intensity as shown in Fig. 1. A metal cathode photodiode[24] monitored the incident beam intensity.

Gaseous N_2 (99.99%) and CO (99.5%) supplied by Matheson were admitted to the sample chamber without further purification. The gas was continuously flowed at 4 l atm/h using an effusive gas capillary array inlet and a throttled turbomolecular pump as an outlet. Sample pressures (5—10 mTorr) were stabilized with a Granville-Phillips leak value servo-locked to an MKS capacitance manometer.

Photoion fluorescence was collected perpendicular to the propagation (X) and polarization (Z) vectors of the vuv excitation (see Fig. 2) through a lens with an accep-

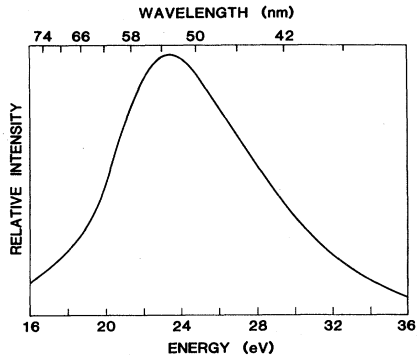

FIG. 1. Relative intensity of the radiation incident on the molecular sample as a function of energy (wavelength).

tance half angle of 8°. The fluorescence passed through an optical train consisting of a polarization analyzer followed by a calcite Glan-Taylor polarizer with its transmission axis along Z. The intensity was measured by a cooled RCA C31000M photomultiplier tube with or without an interference filter. Dark counts averaged about 20 s^{-1}. Standard fast NIM photon counting techniques were employed to measure count rates as low as 300 s^{-1}.

The polarization analyzer permits measurements of fluorescence intensity with the $\vec{E}$ vector parallel (along Z) and perpendicular (along X) to the polarization of the incident light. This was accomplished without mechanical moving parts with a commercial photoelastic modulator (Hinds International PEM CF-4).[25] The PEM contains a CaF_2 crystal that oscillates at its resonant frequency of 50 kHz. This extensional standing wave induces a time-varying uniaxial strain and thus a birefringence in the crystal. When the $\vec{E}$ vector of light is incident at 45° to the PEM crystal birefringent axis, the crystal's oscillation amplitude can be set to provide a sinusoidally varying retardance of amplitude $\lambda_0/2$ and $-\lambda_0/2$ at wavelength λ_0. The time-varying birefringence can be used efficiently to measure the linear polarization of the sample photoion fluorescence.

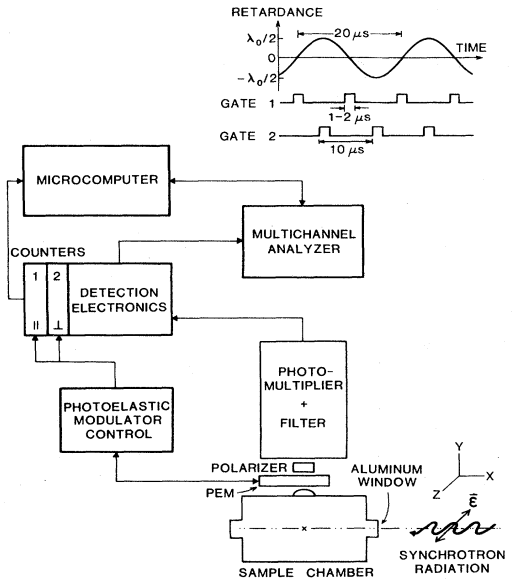

FIG. 2. Schematic layout of the experiment showing the excitation and detection geometry. Inset describes the timing sequence used to measure the polarization of the fluorescence.

Partially linearly polarized light can be described as a superposition of two orthogonal components of linearly polarized light, with random phase. The PEM crystal is followed by a linear polarizer which only passes light polarized along Z. When the time-varying retardance of the PEM passes through zero, as shown in Fig. 2, parallel fluorescence passes onto the detector photomultiplier and the gate is enabled on counter 1. At the $\lambda_0/2$ and $-\lambda_0/2$ extents of the crystal, the gate is enabled on counter 2. The PEM acts as a half-wave plate causing I_X and I_Z to be rotated to the Z and X directions, respectively. Counter 2 thus monitors perpendicular fluorescence intensity. The fluorescence polarization P can be determined from the relation $P=(I_1-I_2)/(I_1+I_2)$, where counter 1 measures I_Z and counter 2 measures I_X. The rapid sampling ($\sim$100 kHz) of this measurement method ensures immunity to fluctuations in gas pressure and light intensity that are slower than about 10 kHz. This is a significant advantage when one is trying to measure precisely total intensity differences on the order of a few percent.

The counter gates open in phase with PEM for 1 to 2 μs every 10 μs. Photon counts at each incident energy were collected until acceptable statistics were attained. Photomultiplier dark counts were measured frequently and they were included in the calculation of P. The background scattered light in the empty chamber was found to be negligible.

Raw polarizations are corrected for finite sample gate width and finite fluorescence bandwidth as outlined in Appendix A. The correction to the polarization for finite solid angle of observation is very small for this experimental configuration (<0.0003 for $P=0.05$, for example).[26] The systematic polarization was checked using a nominally unpolarized light source.[26]

Photoion fluorescence excitation spectra as a function of incident energy were acquired from the total ungated signal by scanning the monochromator. An Ortec time-to-amplitude converter and multichannel analyzer (TAC/MCA) combination measured fluorescence time decays when the storage ring operated with a single 100-ps pulse every 780 ns. From these decays, collisionless radiative lifetimes were determined.

IV. RESULTS

A. N_2^+ B-X fluorescence polarization

The polarization of the total undispersed $N_2^+ B\,^2\Sigma_u^+$-$X\,^2\Sigma_g^+$ fluorescence following photoionization of N_2 is shown in Fig. 3 as a function of excitation energy at 0.28-nm (0.80 to 0.20 eV) and 0.90-nm (0.68 to 0.82 eV) resolution, as noted. The gas sample pressures were 5—10 mTorr. Previous studies have shown that the $v'=0$ level of the $N_2^+ B\,^2\Sigma_u^+$ state contributes more than 90% to the

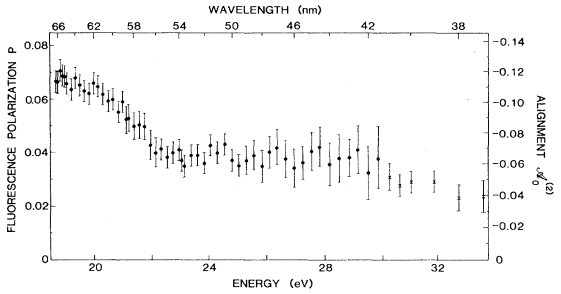

FIG. 3. Degree of polarization P of the $N_2^+ B\,^2\Sigma_u^+$-$X\,^2\Sigma_g^+$ emission and alignment $\mathscr{A}_0^{(2)}$ of $N_2^+ B\,^2\Sigma_u^+$ following photoionization of N_2 by a beam of linearly polarized radiation as a function of incident energy (wavelength). Data taken at 0.28-nm resolution are denoted by closed circles; data at 0.90-nm resolution are denoted by crosses. Error bars represent two standard deviations in the photon counting statistics.

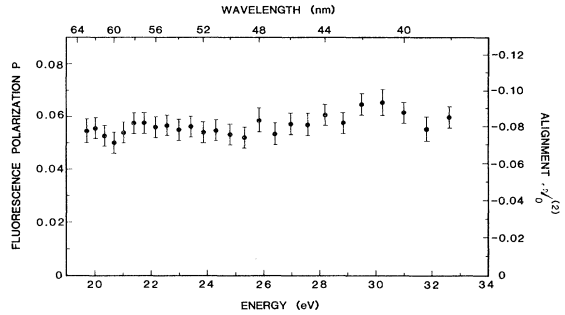

FIG. 4. Degree of polarization P of the $CO^+ B\,^2\Sigma^+$-$X\,^2\Sigma^+$ emission and alignment $\mathscr{A}_0^{(2)}$ of $CO^+ B\,^2\Sigma^+$ following photoionization of CO by a beam of linearly polarized radiation as a function of incident energy (wavelength). All data are taken at 0.90-nm resolution and the error bars represent two standard deviations in the photon counting statistics.

emission in the (350—650)-nm wavelength region while emission from the $v'=1$ level appears to comprise the remaining 10% of the emission.[27,28] Emission from the $N_2^+ A\,^2\Pi_u$-$X\,^2\Sigma_g^+$ band system following photoionization has not been observed at wavelengths shorter than the long-wavelength cutoff of the photomultiplier tube used in this study.[27] Although the $N_2^+ C\,^2\Sigma_u^+$ state can be populated at excitation energies higher than 23.6 eV,[29] its influence on the polarization measurements also can be neglected because the C-X band system lies at wavelength shorter than 200 nm,[29] below the transmission cutoff of the polarization analyzer.

As a check on the identification of the emitting state, the lifetime of the total emission was measured to be 63 ± 2 ns, in good agreement with the known radiative lifetime (61.1 ± 1.1 ns) of the $N_2^+ B\,^2\Sigma_u^+$ state.[30] In addition, the total fluorescence excitation spectrum has a threshold at 18.7 eV in agreement with the observed onset for the production of the $N_2^+ B\,^2\Sigma_u^+$ state.[28]

The polarization values have been corrected for the PEM polarization analyzer gate widths and the measured systematic bias of the detector. As presented, these polarizations are accurate on an absolute scale to ±0.01. Relative uncertainties (two standard deviations) determined by counting statistics are as shown in the figure. When the sample pressure was varied from 5 to 25 mTorr no change in the observed polarization was found, indicating that collisional depolarization of the excited state is negligible under the experimental conditions. Because of the short lifetime of the $N_2^+ B\,^2\Sigma_u^+$ state, depolarization by ambient magnetic fields is also determined to be negligible.[22,31]

B. CO^+ B-X fluorescence polarization

Polarization of $CO^+ B\,^2\Sigma^+$-$X\,^2\Sigma^+$ fluorescence following photoionization is shown in Fig. 4 as a function of excitation energy at 0.90-nm resolution (0.26—0.82 eV). The gas sample pressure was 10 mTorr. An interference filter centered at 22 nm [40 nm full width at half maximum (FWHM)] isolated the $CO^+ B\,^2\Sigma^+$-$X\,^2\Sigma^+$ fluorescence for polarization analysis. The $CO^+ A\,^2\Pi_{3/2,1/2}$ state is also produced from CO photoionization in this energy region. The interference filter is needed to block the strong $CO^+ A\,^2\Pi_{3/2,1/2}$-$X\,^2\Sigma^+$ emission.[32]

Measurements of total fluorescence through the interference filter as a function of excitation energy show an onset of fluorescence at 19.7 eV, which is the energetic threshold for production of the $CO^+ B\,^2\Sigma^+$ state.[33] Low count rates required polarization measurements to be made at a lower resolution than for N_2^+. The interference filter and reduced transmission of the crystal polarizer around 220 nm contribute to a reduction of the observed fluorescence intensity. Additionally, the CO^+ B-X fluorescence production cross section is lower than the N_2^+ B-X fluorescence cross section over the energy range studied.[17]

The same corrections have been made to the CO^+ B-X polarization measurements as for the N_2^+ B-X measurements. The resulting polarizations are accurate on an absolute scale to ±0.01. The $CO^+ B\,^2\Sigma^+$ lifetime lies between 50 and 60 ns,[34] and thus the earth's magnetic field depolarization of the fluorescence once more can be ignored.

V. ANALYSIS

A. N_2 photoionization alignment and channel ratios

The $^{14}N_2$ molecule has two identical nuclei of spin $I=1$. Consequently, hyperfine and spin-rotation coupling effects both need to be considered. In this case, the resultant total nuclear spin $T=0$ and 2 couple to even N of $N_2 X\,^1\Sigma_g^+$ and $T=1$ couples to odd N owing to the (g) inversion symmetry of the ground-state molecular wave functions. Upon photoionization $N_2^+ B\,^2\Sigma_u^+$ is produced, with the requirement that $(N'-N)=\pm1,\pm3,\ldots$. We approximate the population of a rotational level N' in $N_2^+ B\,^2\Sigma_u^+$ to be equal to one-half the sum of the population of the levels $N=N'+1$ and $N=N'-1$ in a thermal nascent $N_2 X\,^1\Sigma_g^+$ sample. Thus $I(N',N'')$ is described by

$$I(N',N'')=\tfrac{1}{2}g(N')(N'+N''+1)\times\{\exp[-B_0(N'+1)(N'+2)/kT]+\exp[-B_0(N'-1)N'/kT]\}\,, \quad (24)$$

where B_0 is the rotational constant for $N_2 X\,^1\Sigma_g^+(v=0)$ and $g(N')$ is a weighting factor for the intensity alternation in emission that results from the restrictions on hyperfine populations described above. The $\bar{g}^{(2)}(N')$ for odd N' in emission are similarly averaged over the relative contributions from the $T=0$ and $T=2$ hyperfine populations such that

$$\bar{g}_{\rm av}^{(2)}(N')=\tfrac{1}{6}[\bar{g}^{(2)}(N')_{(T=0)}+5\bar{g}^{(2)}(N')_{(T=2)}]\ .$$

In Hund's case $b_{\beta S}$, the depolarization factor $g^{(2)}(N')$ is expressed as an average over depolarization factors for the resultants of $\vec{S}'+\vec{I}'$, weighted by their degeneracies. The relevant $\bar{g}_{\rm av}^{(2)}(N')$ for $N'=1$ to 10 are shown in Table I for coupling cases $b_{\beta J}$ and $b_{\beta S}$.

Case $b_{\beta S}$ is considered here because at low N', where the spin-rotation and hyperfine interactions are comparable, the $N_2^+ B\,^2\Sigma_u^+$ angular momentum coupling may be described as intermediate between these two limits. The values for the Fermi-contact constant $b'=630\pm9$ MHz and the spin-rotation constant $\gamma'=450\pm30$ MHz measured recently by Rosner *et al.*[35] verify that the angular momentum coupling at low N' in N_2^+ is intermediate between case $b_{\beta S}$ and $b_{\beta J}$. Such a mixed case can be treated as outlined by Fano and Macek[18] but we find that for a room-temperature sample of N_2 the change introduced into our results using these coupling case limits is small.

In fact, the disalignment induced by the nuclear and electron spin in $N_2^+ B\,^2\Sigma_u^+$ reduces the maximum observable (unresolved) polarization anisotropy at 293 K by about 18% from the classical result. The N'-independent alignment $\mathscr{A}_0^{(2)}$ is presented in Fig. 3 for N_2^+, including corrections for spin and hyperfine depolarization. The values of $\frac{1}{2}(\mathscr{R}_+ + \mathscr{R}_-)$ and $\mathscr{R}_0$ for $N_2^+ B\,^2\Sigma_u^+$ are shown in Table II for coupling case $b_{\beta J}$. Using these quantities, channel ratios for N_2 photoionization are determined from the measured polarizations and are plotted in Fig. 5. Note that the quantum-mechanical depolarization correction *decreases* γ over an analysis using the high-N classical limit. Relative errors are calculated using estimated uncertainties in the polarization and represent two standard deviations.

TABLE I. Depolarization corrections relevant to CO^+ and N_2^+.

N'	Case b[a] $\bar{g}^{(2)}(N')$	Case $b_{\beta J}$[b] $\bar{g}_{\rm av}^{(2)}(N')$	Case $b_{\beta S}$[b] $\bar{g}_{\rm av}^{(2)}(N')$
1	0.333	0.124	0.249
2	0.760	0.374	0.437
3	0.878	0.417	0.447
4	0.926	0.751	0.758
5	0.950	0.679	0.686
6	0.965	0.875	0.877
7	0.973	0.813	0.815
8	0.979	0.926	0.926
9	0.983	0.880	0.880
10	0.986	0.951	0.951

[a]For CO^+ for which $S'=\frac{1}{2}$ and $I'=0$.

[b]For N_2^+ for which $S'=\frac{1}{2}$ and $I_1'=I_2'=1$.

TABLE II. Averaged alignment factors in a Σ-Σ transition.

	High-N' limit	CO^+	N_2^+[a]
$\frac{1}{2}(\mathscr{R}_+ + \mathscr{R}_-)$	0.10	0.098	0.082
$\mathscr{R}_0$	−0.20	−0.187	−0.157

[a]Case $b_{\beta J}$.

B. CO photoionization alignment and channel ratios

The population of a given N' in $CO^+ B\,^2\Sigma^+$ can be approximated to be equal to the population in $N=N'$ of $CO X\,^1\Sigma^+$. Although there are no hyperfine splittings in the $B\,^2\Sigma^+$ state of $^{12}C\,^{16}O$, relatively large spin-rotation splittings occur with $\gamma'=540$ MHz.[36] The depolarization caused by the $\vec{N}\cdot\vec{S}$ interaction can be treated using Eq. (17), which reduces in this case to

$$\bar{g}^{(2)}(N')=\sum_{J'}\frac{(2J'+1)^2}{2S'+1}\begin{Bmatrix} J' & J' & 2 \\ N' & N' & S' \end{Bmatrix}^2 . \qquad (25)$$

Values of $\bar{g}^{(2)}(N')$ for some low N' are listed in Table I.

We find that the maximum positive value of the rotationally averaged polarization anisotropy for CO^+ at $T=293$ K differs by only $\sim2\%$ from the high-N' maximum $\langle R\rangle=\frac{1}{10}$. This agreement is somewhat fortuitous, since the maximum observable polarization anisotropy for CO^+ B-X is 0.106 ($P=0.151$). The value $\langle R\rangle=0.106$ also agrees with an unresolved resonance fluorescence calculation for CO^+ without spin depolarization. Consequently,

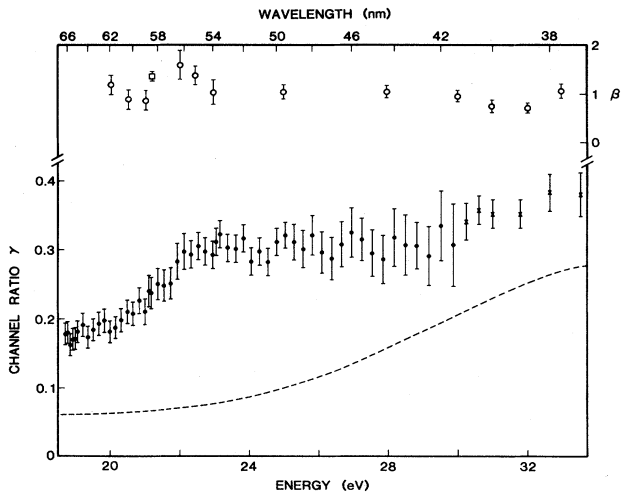

FIG. 5. Plot of the channel ratio γ vs energy (wavelength) of the ionizing radiation for the process $N_2+h\nu \rightarrow N_2^+ B\,^2\Sigma_u^+ + e^-(\epsilon\sigma_g,\epsilon\pi_g)$. Data at 0.28-nm resolution are represented by closed circles, and data at 0.90-nm resolution are represented by crosses; the error bars represent two standard deviations. Also shown by open circles is the data of Marr *et al.* (Ref. 5) for the β parameter; the square at 21.2 eV is the β parameter of Hancock and Samson (Ref. 39) and the dashed curve is the calculation of Rescigno *et al.* (Ref. 14).

the CO^+ spin-rotation depolarization plays no significant role in the present analysis. The alignment of the $CO^+ B\,^2\Sigma^+$ photoion is shown in Fig. 4. Channel ratios γ determined from the CO^+ fluorescence polarization using Eq. (23) are presented in Fig. 6. Relative errors are calculated as for N_2^+.

VI. DISCUSSION

The photoion fluorescence polarizations measured in the present experiments have been converted to both photoion alignments and photoionization channel ratios. The alignment $\mathcal{A}_0^{(2)}$ can be qualitatively interpreted in terms of the information it provides on the spatial distribution of the angular momentum vectors $\vec{N}'$. We find that $\mathcal{A}_0^{(2)}$ is negative for both N_2^+ and CO^+ photoions. This shows that states with different $|M'|$ are unequally populated, with states of small $|M'|$ predominating. Hence $\vec{N}'$ preferentially points in a direction perpendicular to the $\vec{E}$ vector of the exciting radiation.

The channel ratio γ is a quantitative specification of the parity-favored and -unfavored photoionization pathways, which, in turn, can be related to the $(\epsilon\sigma,\epsilon\pi)$ continuum electron ejection channels, as outlined in Appendix B. Such a relationship permits a comparison of the present experiments to theoretical studies that predict partial cross sections for these continuum electron ejection processes. The channel ratios determined in our polarization studies serve as a test of the current understanding of the dynamics of photoelectron ejection. In what follows, we compare our experimental results to available calculations of partial channel cross sections and to related experiments. N_2 and CO, being isoelectronic, are expected to have similar photoionization mechanisms. The relative cross-section differences that are prominent in Figs. 5 and 6 can be attributed to the additional photoionization pathways available to CO because it lacks inversion symmetry.

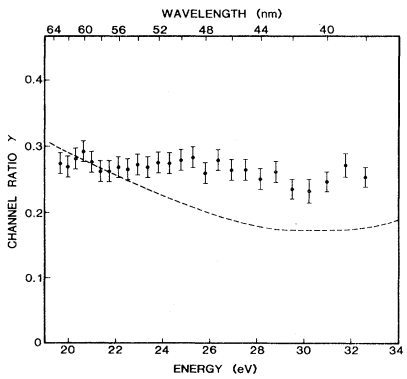

FIG. 6. Plot of the channel ratio γ vs energy (wavelength) of the ionizing radiation for the process $CO + h\nu \rightarrow CO^+ B\,^2\Sigma^+ + e^-(\epsilon\sigma,\epsilon\pi)$ at 0.90-nm resolution. Error bars represent two standard deviations. Dashed curve is from the calculation of Padial *et al.* (Ref. 41).

A. N_2 photoionization

Photoejection of the $3\sigma_g$ and $1\pi_u$ outer electrons of N_2 is reasonably well accounted for theoretically.[14–16] The $2\sigma_u$ ejection leading to $N_2^+ B\,^2\Sigma_u^+$ is by comparison a relatively weak process, in part due to strong $2\sigma_u$ discrete transitions which "rob" oscillator strength from the continuum. The partial cross sections for production of $N_2^+ B\,^2\Sigma_u^+$ as measured by photoelectron[11,12] and fluorescence[17] techniques are well described by Stieltjes-Tchebycheff moment theory (STMT)[14] and frozen-core Hartree-Fock theory.[16]

In N_2, photoejection of the $2\sigma_u$ electron is known to be primarily direct. The very weak Codling series[37] around 23 eV are the only assigned autoionizing resonances that appear in the $N_2^+ B\,^2\Sigma_u^+$ partial cross section. In addition, some weak structure appears in the absorption cross section just above threshold[38] but its origin is unidentified. Note that the σ_u (f-wave) shape resonance which affects the $X\,^2\Sigma_g^+$ cross section cannot be accessed by the $2\sigma_u$ electron owing to symmetry restrictions. Nevertheless, the theoretical calculation of the $2\sigma_u$ β parameter as a function of energy disagrees markedly with experiment.[15,16] The present and previous[10] polarization studies of N_2 yield channel ratios γ that indicate a significantly larger partial cross section for parity-unfavored electron ejection that can be reproduced theoretically. Figure 5 compares our experimental channel ratios to the theories of Rescigno *et al.*[14] using the procedure outlined in Appendix B to convert their calculated σ and π photoelectron ejection cross sections to the channel ratio γ. Rescigno *et al.* calculate a very strong $(2\sigma_u)X\,^1\Sigma_g^+$-$(3\sigma_g)b\,^1\Pi$ valence transition ($f \sim 3.75$) which is borne out reasonably well by experiment.[38] In a one-electron picture, this discrete transition reduces the π continuum channel (and hence γ), particularly at threshold. They note that electron correlations must be considered in order to describe properly the partial channel cross sections. More recent work[16] predicts a value for γ even lower at threshold, with the same general upward trend at higher energies. It appears that present theory is unable to give a satisfactory description of either the channel ratio γ or the β parameter[15] for the photoejection of the $2\sigma_u$ electron in N_2.

Referring again to our data of Fig. 5, we find that γ increases approximately monotonically from 20 to 22 eV and then levels off. This rise corresponds to no obvious variations in the measured partial cross section for $N_2^+ B\,^2\Sigma_u^+$ production. It does, however, coincide with an unexplained resonance that Marr *et al.*[5] found in the $2\sigma_u$ β parameter at about 22 eV, corroborating their indications that at around 22 eV a multielectron excitation process may occur. These data (open circles) are presented with our channel ratios in Fig. 5 for comparison, along with the β parameter of Hancock and Samson[39] at 21.2 eV (open square).

B. CO photoionization

The removal of a 4σ electron from CO to give $CO^+ B\,^2\Sigma^+$ corresponds to the case just discussed for N_2. The CO^+ B-X fluorescence excitation cross section is broad and nearly featureless.[17] Codling and Potts[40] have

examined very weak autoionizing resonances in CO absorption at ~23.5 eV, but these resonances are too weak to be observed in this study. Padial *et al.*[41] find from STMT a strong discrete transition from the ground state $(4\sigma)^1\Sigma^+$ to $(3\pi)^1\Pi$ ($f \sim 0.36$). This theoretical oscillator strength is about half that for the analogous transition in N_2, so that the continuum 4σ-$\epsilon\pi$ STMT cross section is larger than the corresponding $2\sigma_u$-$\epsilon\pi_g$ cross section for N_2. The theoretical 4σ-$\epsilon\sigma$ cross section experiences a maximum at ~32 eV because of a σ (f-wave) shape resonance that couples to the ionization continuum. $CO^+ B\,^2\Sigma^+$ partial cross-section data[12,17] support the existence of this shape resonance.

The STMT calculations predict the channel ratios to have a shallow minimum at about 29—31 eV, as shown in Fig. 6. Our data are remarkably featureless throughout the entire energy region studied, with only perhaps a slight decrease at 30 eV. Thus we find that the σ shape resonance, which affects the cross section for the total $B\,^2\Sigma^+$ state, leaves the partial channel ratios unchanged. This indicates that the partial channel cross sections increase proportionately, an effect that is not predicted theoretically. Nonetheless, the theoretical channel ratio is in fair overall agreement with the experimental data.

C. Concluding remarks

Photoion fluorescence polarization measurements are limited at this time to the study of processes that produce excited-state ions. These are, in the case of N_2 and CO, electron ejections that are difficult to understand theoretically, as judged by the comparison of calculated and experimentally determined partial channel ratios. As such, the present CO study and the extension of the N_2 work provide more stringent information to guide theory. The new N_2 data in particular points out a possible resonance in the $(2\sigma_u)$ channel at 21—22 eV, which was previously suspected from the electron angular distribution data.[5]

We note that fluorescence depolarization caused by electron and/or nuclear-spin angular momentum in the photoion can have important ramifications for photoionization studies of molecules in low-N states (i.e., in supersonic expansions). Depending on the molecule, the maximum observed alignment of photoion product states of low N' can be dramatically *reduced* from the alignment that would be expected in the absence of these spins. Additionally, the quantitative correction for spin-rotation and hyperfine depolarization requires knowledge of the relevant coupling constants in the ion at low N'. It is then likely that a cooled gas sample often may *not* be an advantage for photoion alignment studies via this technique. This may be particularly evident if it is desired to extract channel ratios since the determination of γ from the measured alignment is only strictly valid at high N.

ACKNOWLEDGMENTS

We thank J. L. Durant for valuable experimental assistance, and C. H. Greene and M. A. O'Halloran for helpful discussions. E. D. Poliakoff and C. F. Bender have provided useful comments. We are grateful to D. L. Huestis and M. J. Coggiola for the loan of an MCA computer system. The Digital Equipment Corporation PDP-11/40 computer used to analyzed the fluorescence lifetime data was purchased by SRI International under the National Science Foundation Grant No. NSF-PHY-76-14436. The experiments were performed at the Stanford Synchrotron Radiation Laboratory, which was supported by the U.S. Department of Energy, Office of Basic Energy Sciences, and the National Science Foundation Division of Materials Research. This work was supported by the National Science Foundation under Grants Nos. NSF-PHY-79-08694 and NSF-PHY-06400. One of us (R.N.Z.) also gratefully acknowledges support through the Shell Distinguished Chairs program, funded by the Shell Companies Foundation, Inc.

APPENDIX A: CORRECTIONS TO POLARIZATIONS MEASURED WITH THE PHOTOELASTIC MODULATOR

The photoelastic modulator (PEM) employed in these experiments as part of a polarization analyzer is a commercial device that is commonly used for magnetic circular dichroism and ellipsometry studies.[25] Its application to fluorescence detection is less usual. We have found that the PEM in polarization analysis provides a precise and convenient nonmechanical method to measure small intensity differences in weak fluorescence signals with immunity from most pressure and light-intensity fluctuations. However, the PEM has the disadvantage of a necessary reduction in signal because of the choice of gate widths. Additionally, we need to correct the polarization data for finite detection fluorescence bandwidth and for the depolarizing effect of the finite detector gate width.

1. Correction for finite fluorescence bandwidth

The PEM behaves as a $\lambda/2$ plate at effectively only a single wavelength, determined by the crystal's longitudinal compression. The molecular ion fluorescence monitored here has a 100-Å or more bandwidth depending on the interference filter used before the detector, so the effect of bandwidth should be considered.

The uniaxially strained crystal of the PEM exhibits a time-varying phase retardance. For half-wave (π) retardation at λ_0, the time-dependent retardance $\phi(t)$ at λ can be expressed as

$$\phi(t) = \left[\frac{\pi}{2}\frac{\lambda_0}{\lambda}\right]\sin(\omega t)\,, \tag{A1}$$

where ω is the modulation frequency. As the crystal's zero-crossing, $\sin(\omega t)=0$ and there is no phase retardance at any λ. At the half-wave points, $|\sin(\omega t)|=1$, and $\phi=\pi\lambda_0/2\lambda$. For simplicity, the zero crossings will be referred to as the parallel ($\|$) direction, and the half-wave points as the perpendicular ($\perp$) direction, with reference to the analysis polarizer (Fig. 2). The fluorescence light, which can be considered to be an incoherent superposition of $I_\|$ and $I_\perp$, is described by

$$I_{||}(\omega t)=I_{||}\cos^2\left[\left[\frac{\pi}{2}\frac{\lambda_0}{\lambda}\right]\sin(\omega t)\right],$$
$$I_{\perp}(\omega t)=I_{\perp}\sin^2\left[\left[\frac{\pi}{2}\frac{\lambda_0}{\lambda}\right]\sin(\omega t)\right], \quad \text{(A2)}$$

when the analysis polarizer projects these components.[42] Figure 7 illustrates the variation of $I_{||}(\omega t)$ and $I_{\perp}(\omega t)$ with ωt. The quantity $I_{||}(\omega t)+I_{\perp}(\omega t)$ is normalized to unity at all times.

Since only $I_{\perp}$ is affected by $\lambda\neq\lambda_0$ at its maxima, then

$$I_{\perp}^{\text{obs}}\left[\omega t=\frac{\pi}{2}\right]=I_{\perp}\sin^2\left[\frac{\pi}{2}\frac{\lambda_0}{\lambda}\right]+I_{||}\cos^2\left[\frac{\pi}{2}\frac{\lambda_0}{\lambda}\right],$$
$$I_{||}^{\text{obs}}(\omega t=0)=I_{||}, \quad \text{(A3)}$$

where $I_{||}$ and $I_{\perp}$ refer to the *true* intensity values. Inserting (A3) into the expression for P, we find that

$$P=P_{\text{obs}}\Big/\left[\sin^2\left[\frac{\pi}{2}\frac{\lambda_0}{\lambda}\right]-P_{\text{obs}}\cos^2\left[\frac{\pi}{2}\frac{\lambda_0}{\lambda}\right]\right], \quad \text{(A4)}$$

where P is the true polarization and P_{obs} is measured polarization. Similarly, if $I_{||}$ is taken to be the $\pm\lambda/2$ point, then

$$P=P_{\text{obs}}\Big/\left[\sin^2\left[\frac{\pi}{2}\frac{\lambda_0}{\lambda}\right]+P_{\text{obs}}\cos^2\left[\frac{\pi}{2}\frac{\lambda_0}{\lambda}\right]\right]. \quad \text{(A5)}$$

For the small values ($\sim$0.05) of polarization observed in the present work, Eqs. (A4) and (A5) differ little as shown in Fig. 8, which plots P as a function of emission wavelength for an observed polarization of 0.05 when λ_0 is set at 400 nm. P_{obs} is a slowly varying function of λ, particularly to the long wavelength side of λ_0. In the present experiments no correction is required for the variation of P with fluorescence bandwidth.

In general, spot checks can be made to estimate whether the polarization correction is significant. If the fluorescence monitored is spread over a large spectral region,

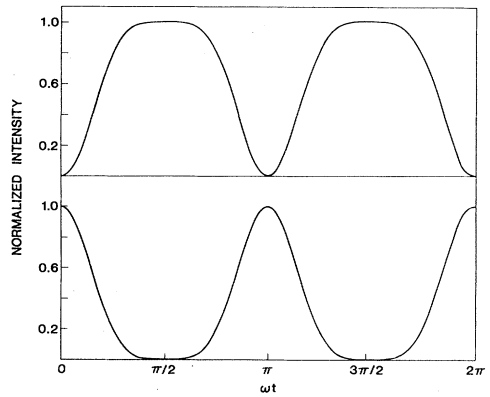

FIG. 7. Variation of $I_{||}(\omega t)$ (lower trace) and $I_{\perp}(\omega t)$ (upper trace) with ωt for a full 2π cycle following Eq. (A2). $I_{||}(\omega t)+I_{\perp}(\omega t)$ is normalized to unity.

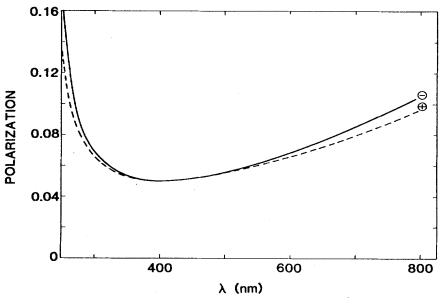

FIG. 8. Polarization P as a function of emission wavelength when the observed polarization $P_{\text{obs}}=0.05$ at λ_0 (the PEM setting) of 400 nm. Solid line is a plot of Eq. (A4) and the dashed line is a plot of Eq. (A5).

then the wavelength varying polarization correction must be changed to that for a polarization anisotropy, R [see Eq. (9)], and integrated over the bandwidth of the emission. Such a large correction is best avoided if quantitative polarizations are needed since product distributions vary with incident excitation energy. Relative photomultiplier quantum efficiency additionally needs to be carefully considered in such cases.

2. Correction for finite gate width of detector

Since the PEM birefringence oscillates sinusoidally at 50 kHz the intensity components $I_{||}$ and $I_{\perp}$ also oscillate in time, as shown in Fig. 7. Ideally, data could be acquired with infinitely narrow gates at the respective crossings, but for an experiment in which the light source is on continuously, this leads to an infinitely small signal. For reasonable gate widths, corrections can be made by reference to Eq. (A2), calling $\lambda=\lambda_0$ for simplicity. A full 2π cycle of ωt is 20 μs for the 50-kHz oscillation. The finite gate width allows some $I_{\perp}$ intensity to spill over into the measured $I_{||}$, and vice versa, i.e.,

$$I_{||}^{\text{obs}}=AI_{||}+(1-A)I_{\perp},$$
$$I_{\perp}^{\text{obs}}=CI_{\perp}+(1-C)I_{||}, \quad \text{(A6)}$$

where

$$A=\int_{-b}^{b}\cos^2\left[\frac{\pi}{2}\sin(\omega t)\right]d(\omega t)/2b,$$

$$C=\int_{\pi/2-b}^{\pi/2+b}\sin^2\left[\frac{\pi}{2}\sin(\omega t)\right]d(\omega t)/2b,$$

and $2b$ is the gate width in radians, which is the fraction of the 2π cycle for which the gate is open multiplied by 2π.

The expressions for A and C must be integrated numerically. Their values for some practical gate widths are shown in Table III. The correction factors are asymmetric, as can be readily intuited from examining Fig. 7.

TABLE III. PEM gate width corrections for $P_{obs}=0.05$.

$2b$	50-kHz crystal gate width (μs)	A	C	$P(I_{\|\|}$ at $0\lambda)$	$P(I_{\|\|}$ at $\pm\frac{1}{2}\lambda)$
0.0	0	1.0	1.0	0.05	0.05
0.050π	0.5	0.9949	1.0	0.0502	0.0503
0.10π	1.0	0.9800	1.0	0.0510	0.0511
0.15π	1.5	0.9560	0.9996	0.0522	0.0524
0.20π	2.0	0.9241	0.9988	0.0540	0.0544
0.25π	2.5	0.8857	0.9971	0.0563	0.0570
0.30π	3.0	0.8425	0.9941	0.0592	0.0603
0.40π	4.0	0.7483	0.9820	0.0674	0.0696
0.50π	5.0	0.6538	0.9581	0.0797	0.0838

The retardance varies more rapidly through the zero crossing than the half-wave points; therefore, the zero-crossing correction predominates. Direct computation of P from P_{obs} is easily performed by evaluating the correction in terms of the ratio

$$\rho=I_{||}/I_{\perp}$$

for which

$$P=(\rho-1)/(\rho+1)\ .$$

We find that

$$\rho=\frac{C\rho_{obs}+A-1}{\rho_{obs}(C-1)+A}\ . \tag{A7}$$

A typical 2-μs gate width causes a correction of about $+0.004$ to an experimental polarization of 0.05. These corrections were applied to our data.

APPENDIX B: RELATION OF THE DIPOLE STRENGTH RATIO D_π^2/D_σ^2 TO γ

In photoionization of molecules, it is conceptually useful to describe the partial channel contributions in terms of the projection k of $\vec{j}_{ph}$ on the molecular axis, which can be 0 or ±1 for a dipole transition. For the N_2 and CO photoionization processes studied here in which a $^1\Sigma^+$ ground state yields a $^2\Sigma^+$ photoion, the projection m_l on the molecular axis of the ejected electron with angular momentum $\vec{\ell}$ must also be 0 or ±1. These are called σ or π photoelectrons, respectively. Unfortunately, photoion fluorescence polarizations do not lead themselves to a simple separation in terms of a ratio of σ and π continuum cross sections in the angular momentum transfer formalism. In fact, Poliakoff *et al.*[10] find that at very low N the dipole strengths

$$D_\sigma^2=\sum_l |D_{l00}^{(-)}|^2$$

and

$$D_\pi^2=\sum_l (|D_{l11}^{(-)}|^2+|D_{l-1-1}^{(-)}|^2)$$

(where the $D_{lkm_l}^{(-)}$ are calculated in the axial recoil approximation for incoming-wave normalized continuum functions[43,44]) cannot be determined from a fluorescence polarization measurement. This is because the interference terms $D_{lkm_l}^{(-)}D_{lk'm'_l}^{(-)}$ ($k\neq k'$, $m_l\neq m'_l$) become significant at low N. This situation contrasts with the complete separability at all N' of the description of photoion alignment in terms of the three channel probabilities $|S(N';j_t)|^2$.

In order to relate the dipole strengths D_σ^2 and D_π^2 to $\mathscr{A}_0^{(2)}(N')$ and hence the amplitudes $|S(N';j_t)|^2$, we must take these models to their high-N limits. By $N=5$, Poliakoff *et al.*[10] find that the dipole amplitude interference terms have nearly disappeared, and the total photoionization cross section can be fully described using only the D_σ^2 and D_π^2 terms. We normalize these dipole strengths so that $\sigma_B D_\sigma^2$ and $\sigma_B D_\pi^2$ (where σ_B is the cross section for the production of the excited N_2^+ or CO^+ photoion in its B state) are the partial cross sections for σ and π photoelectron ejection, respectively, leading to the B state of the ion. At high N, the σ photoelectron ejection can be identified with a purely parallel-type transition. The π photoelectron channel from a $^1\Sigma^+$ molecular ground state can likewise be identified with a weighted average of parallel and perpendicular-type transitions, based on rotational line strengths for Σ-Π absorption.[45] This results in the relation

$$\mathscr{A}_0^{(2)}\simeq\frac{1}{5}\frac{(-2D_\sigma^2+D_\pi^2)}{D_\pi^2+D_\sigma^2} \tag{B1}$$

when the $\mathscr{A}_0^{(2)}(N';j_t)$ in Eq. (5) are replaced by their high-N' limits. Comparison of Eq. (B1) to Eq. (15) permits in the high-N' limit the identification

$$\frac{D_\pi^2}{D_\sigma^2}=\frac{2\gamma}{1-\gamma}\ , \tag{B2}$$

where γ is the channel ratio defined in Eq. (14). The dipole strength ratio D_π^2/D_σ^2 can vary from 0 to ∞, but in this case the channel ratio γ here has a more limited range of 0 to 1.

The polarization anisotropy R can now be written as

$$R=\frac{1}{20}\frac{(2-D_\pi^2/D_\sigma^2)}{(1+D_\pi^2/D_\sigma^2)}\ . \tag{B3}$$

Additionally, by using the normalization condition $\mathscr{S}_+ + \mathscr{S}_0 + \mathscr{S}_- = 1$, the channel probabilities can be reexpressed in terms of the partial channels D_σ^2 and D_π^2:

$$\mathscr{S}_0 = \frac{1}{2}\left[\frac{D_\pi^2}{D_\pi^2 + D_\sigma^2}\right] \tag{B4}$$

and

$$(\mathscr{S}_+ + \mathscr{S}_-) = \frac{1}{2}\left[\frac{2D_\sigma^2 + D_\pi^2}{D_\pi^2 + D_\sigma^2}\right]. \tag{B5}$$

Thus in the limit of high N, the partial cross sections for σ and π photoejection can be directly determined from the normalized angular momentum transfer channel probabilities in the GZ formulation.

*Present address: Department of Physics and Astronomy, Howard University, Washington, D. C. 20059.

[1]J. A. R. Samson, in *Handbuch der Physik,* edited by W. Mehlhorn (Springer, Berlin, 1982), Vol. 31, pp. 123–213.

[2]A. F. Starace, in *Handbuch der Physik,* edited by W. Mehlhorn (Springer, Berlin, 1982), Vol. 31, pp. 1–121.

[3]J. Cooper and R. N. Zare, J. Chem. Phys. 48, 942 (1968); in *Lectures in Theoretical Physics,* edited by S. Geltman, K. T. Mahanthappa, and W. E. Brittin (Gordon and Breach, New York, 1969), Vol. XI-C, pp. 317–37.

[4]J. Berkowitz, *Photoabsorption, Photoionization and Photoelectron Spectroscopy* (Academic, New York, 1979).

[5]G. V. Marr, J. M. Morton, R. M. Holmes, and D. G. McCoy, J. Phys. B 12, 43 (1979).

[6]C. D. Caldwell and R. N. Zare, Phys. Rev. A 16, 255 (1977).

[7]W. Mauser and W. Mehlhorn, in Extended Abstracts of the XIth International Conference on Vacuum Ultraviolet Radiation Physics, Charlottesville, Virginia, 1980 (unpublished), Vol. II, pp. 1–3.

[8]C. H. Greene and R. N. Zare, Phys. Rev. A 25, 2031 (1982).

[9]C. H. Greene and R. N. Zare, Ann. Rev. Phys. Chem. 33, 119 (1982).

[10]E. D. Poliakoff, J. L. Dehmer, D. Dill, A. C. Parr, K. H. Jackson, and R. N. Zare, Phys. Rev. Lett. 46, 907 (1981).

[11]P. R. Woodruff and G. V. Marr, Proc. R. Soc. London Ser. A 358, 87 (1977).

[12]E. W. Plummer, T. Gustafsson, W. Gudat, and D. E. Eastman, Phys. Rev. A 15, 2339 (1977).

[13]J. W. Davenport, Phys. Rev. Lett. 36, 945 (1976).

[14]T. N. Rescigno, C. F. Bender, B. V. McKoy, and P. W. Langhoff, J. Chem. Phys. 68, 970 (1978).

[15]S. Wallace, D. Dill, and J. L. Dehmer, J. Phys. B 12, L417 (1979).

[16]R. R. Lucchese, G. Raseev, and V. McKoy, Phys. Rev. A 25, 2572 (1982).

[17]L. C. Lee, J. Phys. B 10, 3033 (1977).

[18]U. Fano and J. H. Macek, Rev. Mod. Phys. 45, 553 (1973).

[19]U. Fano and D. Dill, Phys. Rev. A 6, 185 (1972).

[20]D. Dill and U. Fano, Phys. Rev. Lett. 29, 1203 (1972).

[21]D. Dill (private communication).

[22]C. H. Townes and A. L. Schawlow, *Microwave Spectroscopy* (Dover, New York, 1975).

[23]V. Rehn, A. D. Baer, J. L. Stanford, D. S. Kyser, and V. O. Jones, in *VUV Radiation Physics,* edited by E. E. Koch, R. Haensel, and C. Kunz (Pergamon, Braunschweig, 1974), p. 780.

[24]R. B. Cairns and J. A. R. Samson, J. Opt. Soc. Am. 56, 1568 (1966).

[25]J. C. Kemp, J. Opt. Soc. Am. 59, 950 (1969).

[26]K. H. Jackson, Ph.D. thesis, Stanford University (1981) (unpublished).

[27]D. L. Judge and G. L. Weissler, J. Chem. Phys. 48, 4590 (1968).

[28]Wm. B. Peatman, B. Gotchev, P. Gürtler, E. E. Koch, and V. Saile, J. Chem. Phys. 69, 2089 (1978).

[29]A. Lofthus and P. H. Krupenie, J. Phys. Chem. Ref. Data 6, 113 (1977).

[30]F. Remy and M. N. Dumont, J. Quant. Spectrosc. Radiat. Transfer 20, 217 (1978).

[31]A. C. G. Mitchell and M. W. Zemansky, *Resonance Radiation and Excited Atoms* (Cambridge University Press, London, 1961).

[32]D. L. Judge and L. C. Lee, J. Chem. Phys. 57, 455 (1972).

[33]M. Ogawa and S. Ogawa, J. Mol. Spectrosc. 41, 393 (1972).

[34]S. W. Jørgensen and G. Sørensen, J. Chem. Phys. 62, 2550 (1975).

[35]S. D. Rosner, T. D. Gaily, and R. A. Holt, Phys. Rev. A 26, 697 (1982).

[36]K. P. Huber and G. Herzberg, *Molecular Spectra and Molecular Structure IV. Constants of Diatomic Molecules* (Van Nostrand Reinhold, New York, 1979).

[37]K. Codling, Astrophys. J. 143, 552 (1966).

[38]P. Gürtler, V. Saile, and E. E. Koch, Chem. Phys. Lett. 48, 245 (1977).

[39]W. H. Hancock and J. A. R. Samson, J. Electron Spectrosc. Relat. Phenom. 9, 211 (1976).

[40]K. Codling and A. W. Potts, J. Phys. B 7, 163 (1974).

[41]N. Padial, G. Csanak, B. V. McKoy, and P. W. Langhoff, J. Chem. Phys. 69, 2992 (1978).

[42]W. A. Shurcliff and S. S. Ballard, *Polarized Light* (Van Nostrand, Princeton, 1964).

[43]J. L. Dehmer and Dan Dill, Phys. Rev. A 18, 164 (1978).

[44]The treatment of Refs. 10 and 43 defines D_π^2 as $\sum_l |D_{l-1-1}^{(-)}|^2$ *or* $\sum_l |D_{l1}^{(-)}|^2$. Thus the D_π^2 of the present work is equal to *twice* the D_π^2 used by Poliakoff *et al.* (Ref. 10) and Dehmer and Dill (Ref. 43).

[45]G. Herzberg, *Molecular Spectra and Molecular Structure I. Spectra of Diatomic Molecules* (Van Nostrand Reinhold, New York, 1950).